Supporting Information

Regulating Intermolecular Interactions for Stable Multifunctional Organic-Inorganic Metal Halide Hybrid Glasses

Chunyan Jiang, Jing Yan, Jianrong Qiu, Mingmei Wu, and Beibei Xu**

Experimental Section

Materials. $SbCl_3$ (99%), 1-benzyl-3-methylimidazolium chloride (BzmimCl, 99%), 1-butyl-3-methylimidazolium chloride (BmimCl, 99%), 1-butyl-2,3-dimethylimidazolium chloride (BmmimCl, 99%), N, N-dimethylformamide (DMF), ethanol, and diethyl ether were purchased from Macklin Reagent Company and used without further purification.

Synthesis of $Bzmim_3SbCl_6$ single crystal. 2 mmol $SbCl_3$ and 6 mmol BzmimCl were weigh and dissolved with 5 mL DMF in a glass bottle. With stirring for 20 min, a clear solution was formed. After filtration with disposable filter, the solution was collected in a glass bottle. With its lid open, the bottle was then placed in a closed chamber filled with diethyl ether. Colorless transparent single crystals of $Bzmim_3SbCl_6$ were obtained through vapor diffusion of diethyl ether into this solution after an overnight period. The crystals were washed with diethyl ether in vacuum filtration devices and dried under reduced pressure at 60 ℃ for 6h.

Synthesis of $Bzmim_2SbCl_5$ single crystal. The synthesis of $Bzmin_2SbCl_5$ single crystals was the same with that of $Bzmin_3SbCl_6$ single crystals except that stoichiometric ratio of 2 mmol $SbCl_3$ and 4 mmol BzmimCl were used. After two days, yellow transparent $Bzmin_2SbCl_5$ single crystals were obtained. The crystals were washed with diethyl ether and dried under reduced pressure at 60 ℃ for 6h.

Synthesis of $Bzmim_3SbCl_6$ Glass. The $Bzmim_3SbCl_6$ Glass was prepared by melt-quenching method. Quartz dish was cleaned by ultrasonic with isopropyl alcohol and ultrapure water in sequence, and then it was dried under reduced pressure. $Bzmim_3SbCl_6$ crystal powders were placed in the cleaned quartz dish and heated in hot plate, with holding at 160 ℃ for 10 min. A molten liquid was obtained, and it was removed and placed in room temperature. Glass was

formed after several mins.

Synthesis of $Bzmim_2SbCl_5$ Glass. The $Bzmim_2SbCl_5$ glass was prepared by the same melt-quenching method. $Bzmim_2SbCl_5$ crystal powders were placed in the cleaned quartz dish and then heated in hot plate at 120 ℃ for 10 min. The molten liquid was removed and placed in room temperature. Glass was formed after several mins.

Synthesis of $Bzmim_2SbCl_5$ Glass Ceramic. The $Bzmim_2SbCl_5$ glass ceramic was prepared by open environment annealing treatment of $Bzmim_2SbCl_5$ glass. The $Bzmim_2SbCl_5$ glass were placed in hot plate, after holding at 90 ℃ for 3h, transparent glass ceramic was obtained.

Synthesis of $Bmim_2SbCl_5$ single crystal. 3 mmol $SbCl_3$ and 6 mmol BmimCl were weigh and dissolved with 1 mL ethanol in a glass bottle. The mixture was heated in a vial at 70 °C for a duration of 10 minutes, and a transparent, pale yellow solution was yielded. Upon cooling to room temperature, the solution gradually deposited light yellow crystals.

Synthesis of $Bmmim_2SbCl_5$ single crystal. 1 mmol $SbCl_3$ and 2 mmol BmmimCl were weigh and transferred into a 20 mL Teflon-lined autoclave reactor. The autoclave reactor was heated at 120 °C for 24 h. The reactor was cooled naturally to room temperature, and single crystals were obtained.

Characterization. Single crystal X-ray diffraction data was collected on the Agilent SuperNova single crystal diffractometer at 150 K with the Ga Kα (λ= 1.34138 nm) radiation. Powder X-ray diffraction patterns were collected on the Bruker D8 advance diffractometer the Cu Kα (λ=1.54184 nm) radiation at 40 kV and 40 mA. Temperature-dependent powder X-ray diffraction patterns measurements were performed on the Rigaku Smartlab diffractometer equipping with a temperature control sample holder. Thermogravimetry analysis was carried

out on the Netzsch TG 209F1 Libra system at a heating rate of 10 K/min under a nitrogen atmosphere. Differential scanning calorimetry measurement was performed on the TA DSC 2500 instrument at a heating rate of 5-30 K/min and cooling rate of 30 K/min under a nitrogen atmosphere. Raman spectra was recorded on the RENISHAW InVia-Reflex Mciro-Confocal Raman spectrometer using an incident 785 nm laser. X-ray photoelectron spectroscopy was performed by using ESCALAB QXi spectrometer (ThermoFisher Scientific, USA) with non-monochromatic Al Ka X-ray (1486.6 eV) at pass energy of 50 eV and 200 eV to determine the chemical environment of the samples. UV-Vis transmittance and diffuse reflectance spectra were measured on the Cary 5000 UV–vis–near-IR spectrophotometer, and $BaSO_4$ powder was used as the standard reference for diffuse reflectance spectra. Steady state and time resolved photoluminescence spectra were recorded in the Edinburgh FLS1000 spectrometer with 450 W Xenon lamp and 350 nm picoseconds pulsed diode laser with a repetition rate of 10 MHz (100 ns) were used as the excitation source, respectively. Temperature dependent photoluminescence spectra were recorded in the same spectrometer with the equipment of an Oxford cryostat. Luminescence quantum efficiency was acquired in the same spectrometer using $BaSO_4$ coated integrating sphere as sample holder. *In-situ* polarizing optical microscopy images were collected on the Leica DM2700P Microsystems with a homemade temperature control sample stage. Scanning electron microscope images were taken on a JSM-IT200A field emission microscope (JEOL, Japan). The viscosity of melt was measured in a flowing nitrogen atmosphere on a TA ARES-G2 rheometer (TA, USA) with a parallel-plate geometry (20 cm) at shear rate of 10 s^{-1} and 1 s^{-1}. Hirshfeld analysis was conducted on Crystal Explorer program.

Computational details. The initial structures were excised from the corresponding crystal

structure, and hybrid functional B3LYP-D3(BJ) with mixed basis set (def2-SVP for Sb atoms and 6-31G* for all other atoms) were used for hydrogen atoms optimization. All the optimizations were performed on Gaussian 09 program. The symmetry adapted perturbation theory (SAPT) was employed to identify the contribution of electrostatic, exchange, induction, and dispersion items to the total intermolecular interaction energy. The calculation was performed on PSI4 program with SAPT2+(3)δMP2/aug-cc-pVTZ level as implemented in PSI4 program. Moreover, to visualize interactions in OIMH, the independent gradient model based on Hirshfeld partition analysis was carried out with Multiwfn program.

[CCDC 2358246, 2358247 contains the supplementary crystallographic data for this paper. These data can be obtained free of charge from The Cambridge Crystallographic Data Centre via www.ccdc.cam.ac.uk/data_request/cif.]

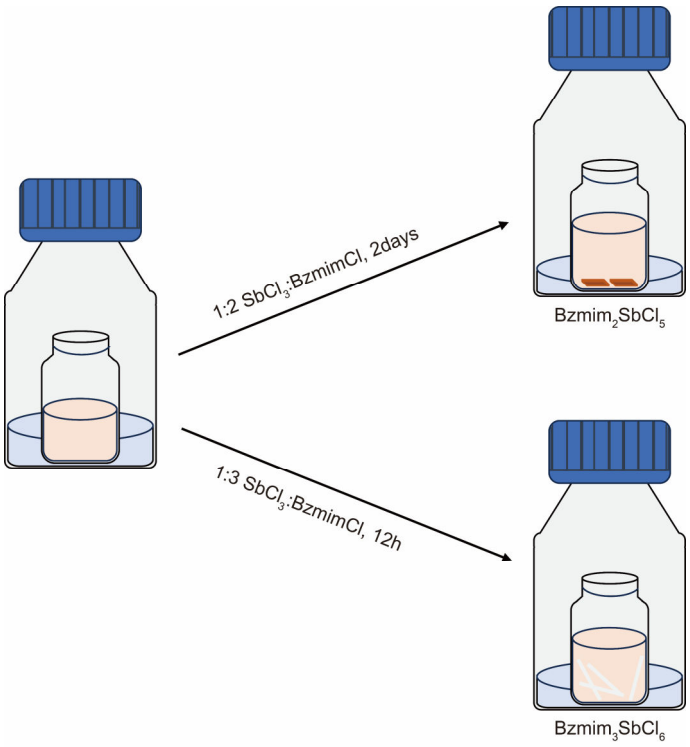

Figure S1. Schematic diagram of a $Bzmim_3SbCl_6$ and $Bzmim_2SbCl_5$ single crystals being grown by anti-solvent diffusion method.

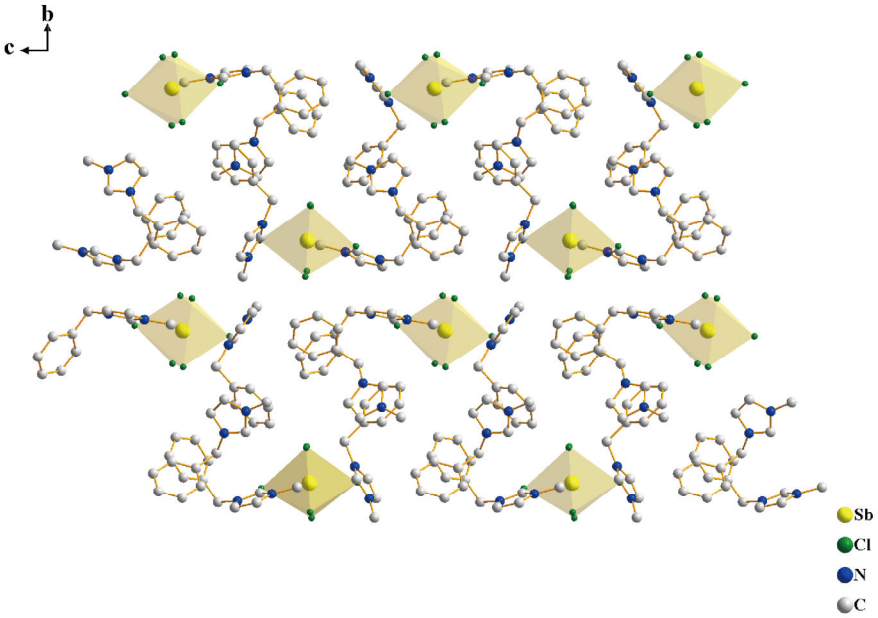

Figure S2. Stacking view of single crystal structure of $Bzmim_3SbCl_6$ from [100].

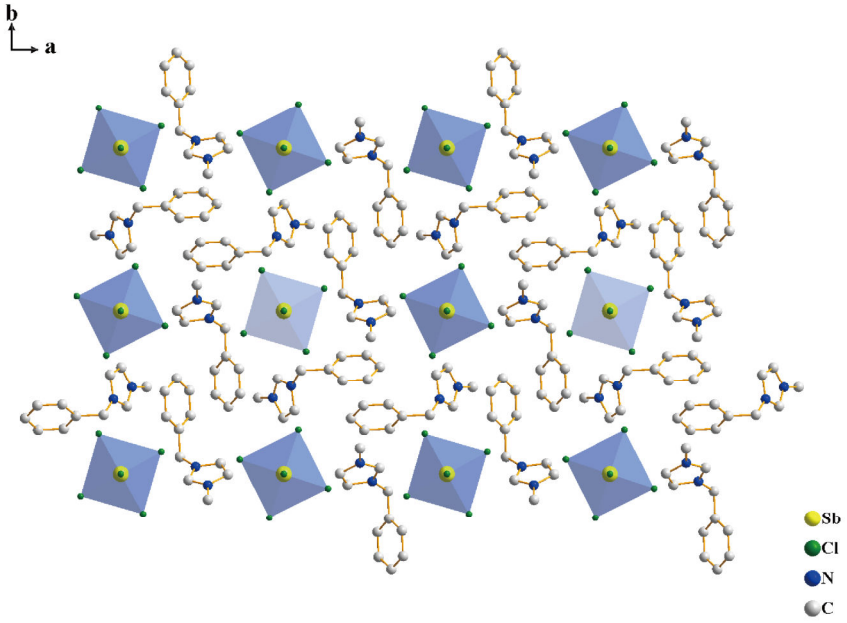

Figure S3. Stacking view of single crystal structure of $Bzmim_2SbCl_5$ from [001].

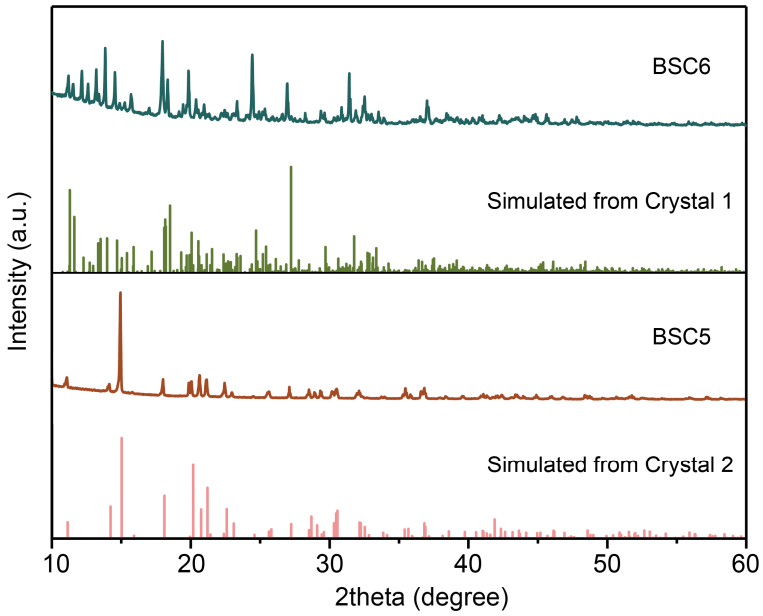

Figure S4. Powder XRD patterns of $Bzmim_3SbCl_6$ and $Bzmim_2SbCl_5$ single crystals.

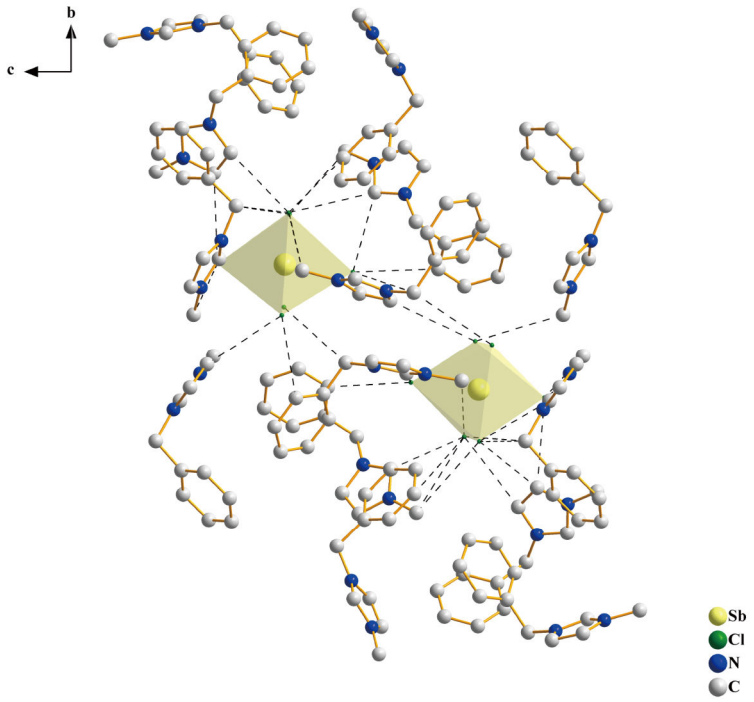

Figure S5. Hydrogen bonds in $Bzmim_3SbCl_6$.

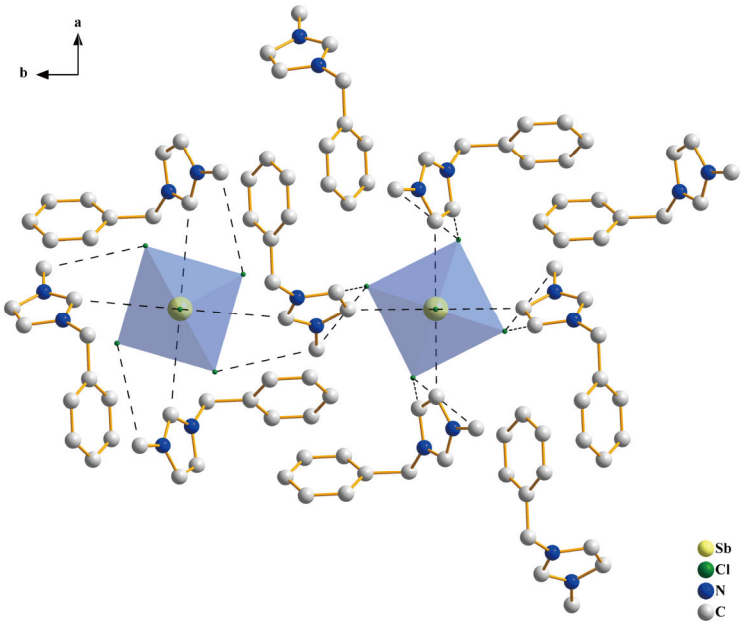

Figure S6. Hydrogen bonds in $Bzmim_2SbCl_5$.

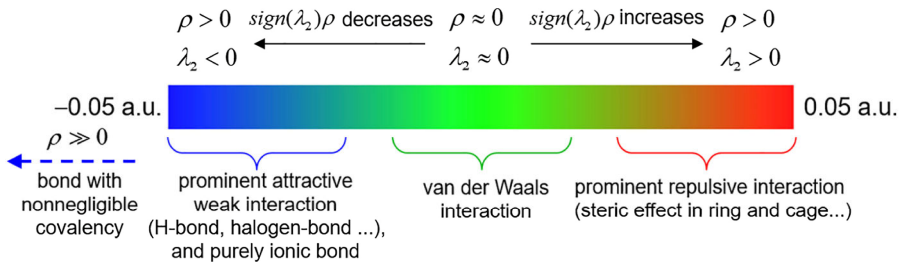

Figure S7. Color-bar of independent gradient model based on Hirshfeld partition (IGMH) analysis.

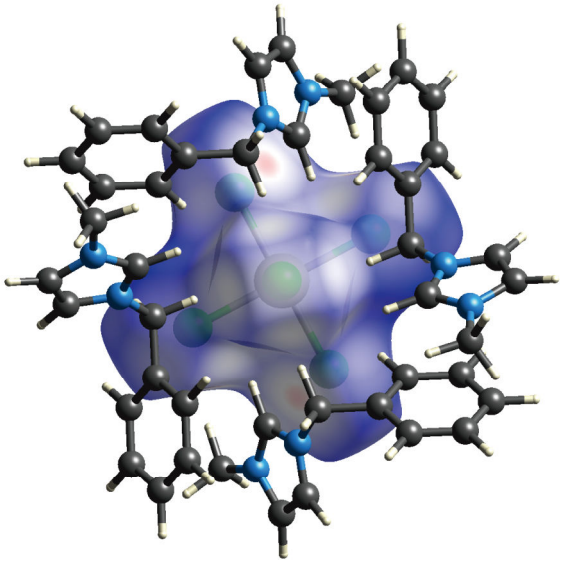

Figure S8. Hirshfeld surfaces of $Sb1Cl_5^{2-}$ surrounded by a cluster of neighboring molecules. Red indicating distances smaller than the van der Waals separation distance, white indicating distances equal to it, and blue indicating distances larger than the van der Waals separation distance.

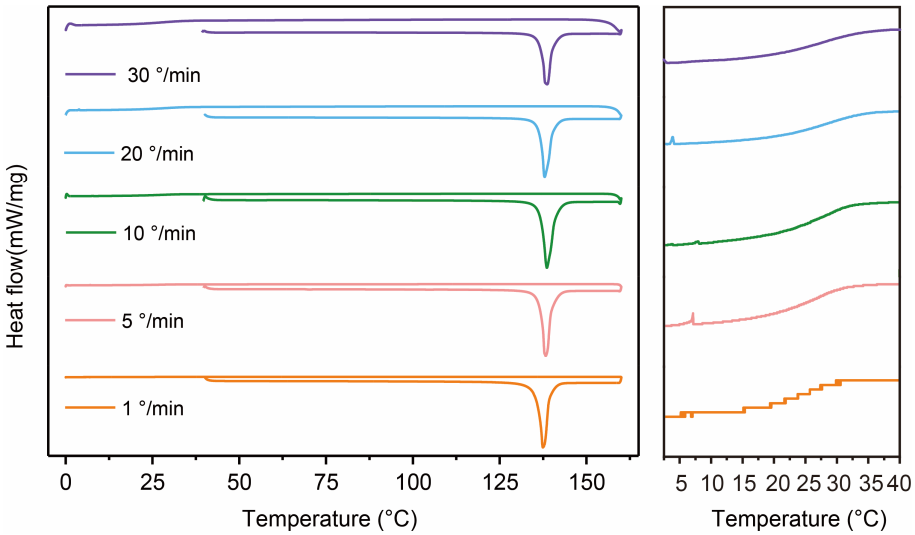

Figure S9. DSC curves of $Bzmim_3SbCl_6$ at heating rate of 20 °/min and cooling rate of 1, 5, 10, 20, 30 °/min.

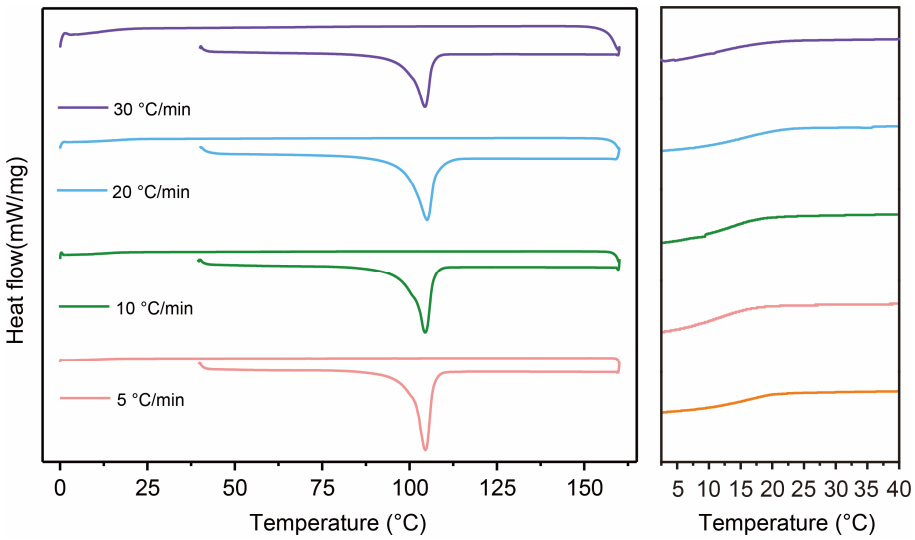

Figure S10. DSC curves of $Bzmim_2SbCl_5$ at heating rate of 20 °/min and cooling rate of 1, 5, 10, 20, 30 °/min.

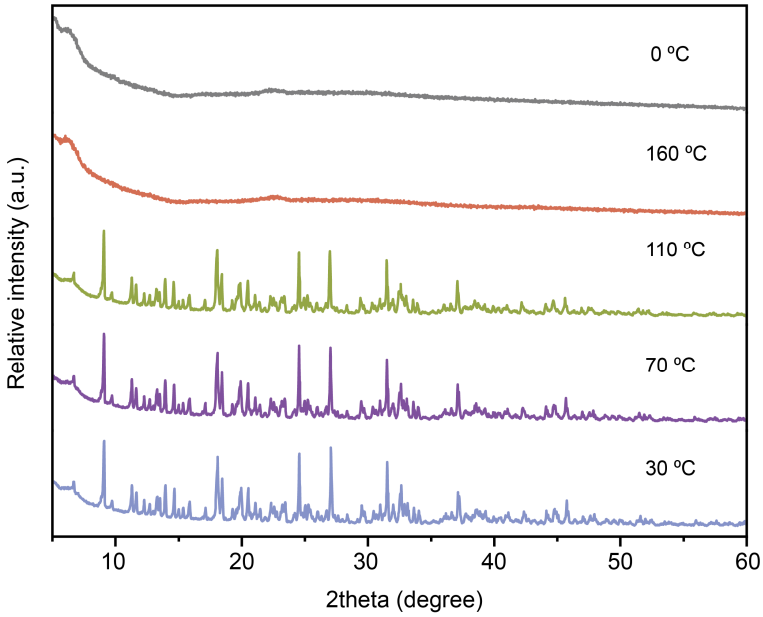

Figure S11. Temperature dependent XRD patterns of $Bzmim_3SbCl_6$.

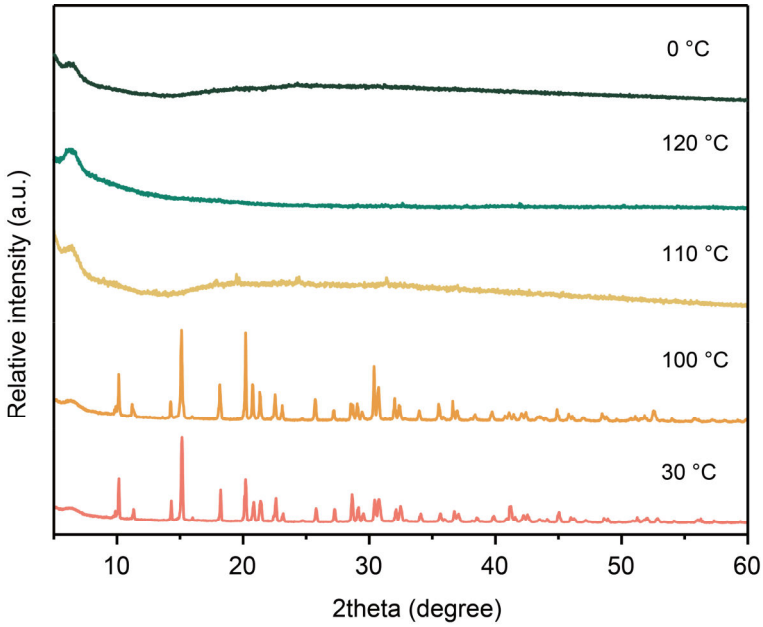

Figure S12. Temperature dependent XRD patterns of $Bzmim_2SbCl_5$.

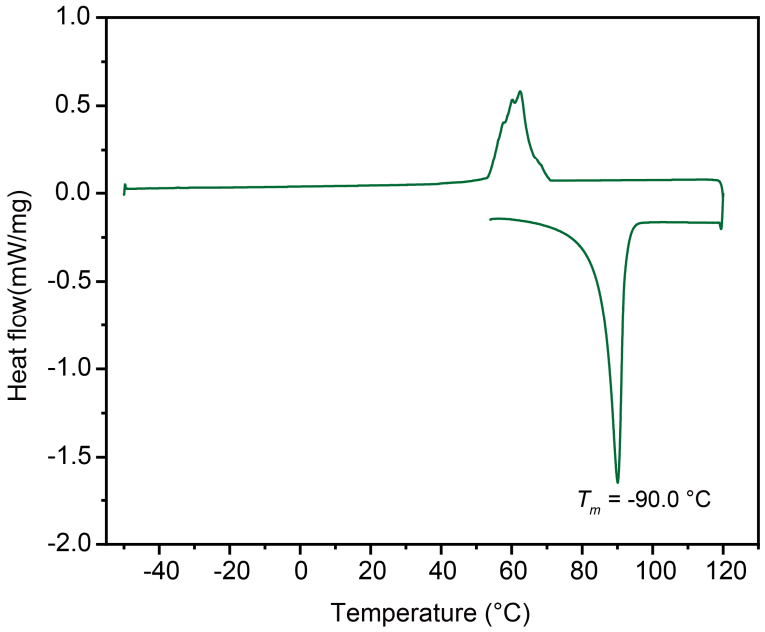

Figure S13. DSC curves of $Bmim_2SbCl_5$ at heating rate of 10 °/min and cooling rate of 10 °/min.

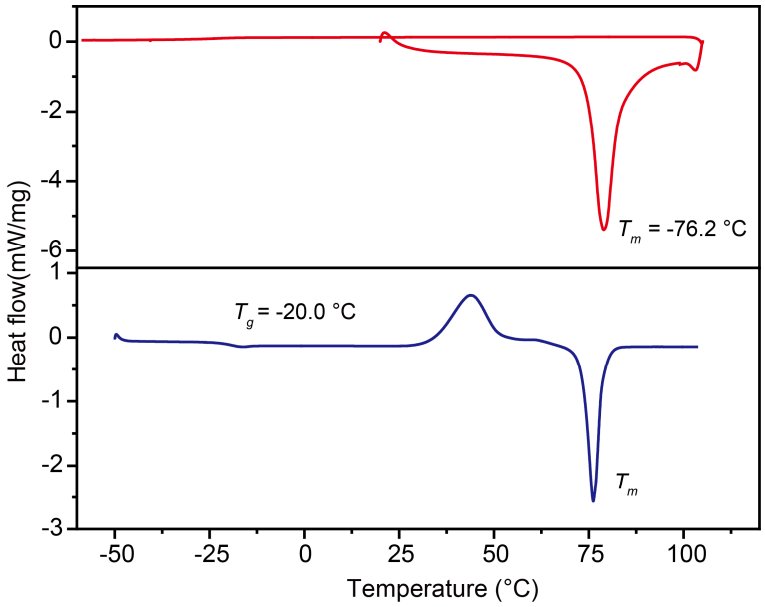

Figure S14. DSC curves of $Bmmim_2SbCl_5$ at heating rate of 10 °/min and cooling rate of 10 °/min.

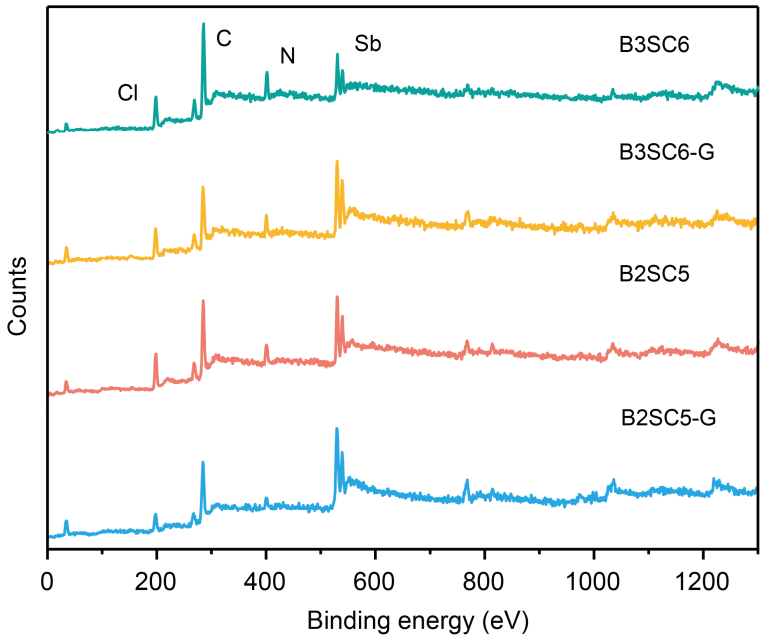

Figure S15. Survey XPS spectra of $Bzmim_3SbCl_6$, $Bzmim_3SbCl_6$ glass, $Bzmim_2SbCl_5$, and $Bzmim_2SbCl_5$ glass.

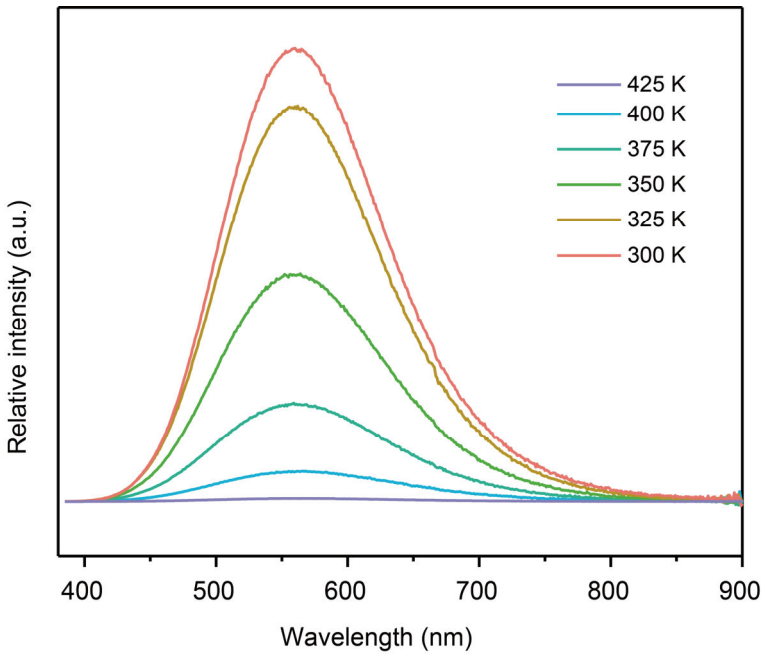

Figure S16. Temperature dependent emission spectra of $Bzmim_3SbCl_6$ (λ_{ex} = 365 nm).

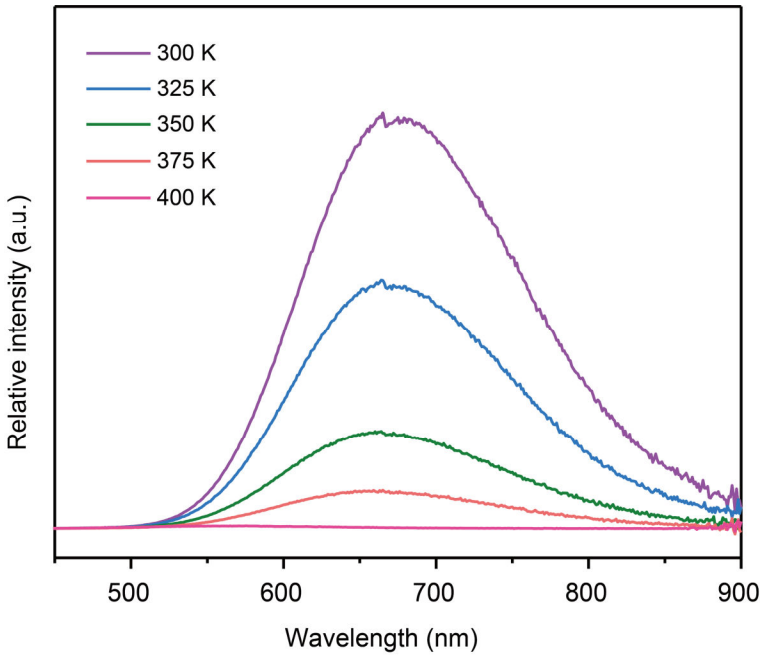

Figure S17. Temperature dependent emission spectra of $Bzmim_2SbCl_5$ (λ_{ex} = 365 nm).

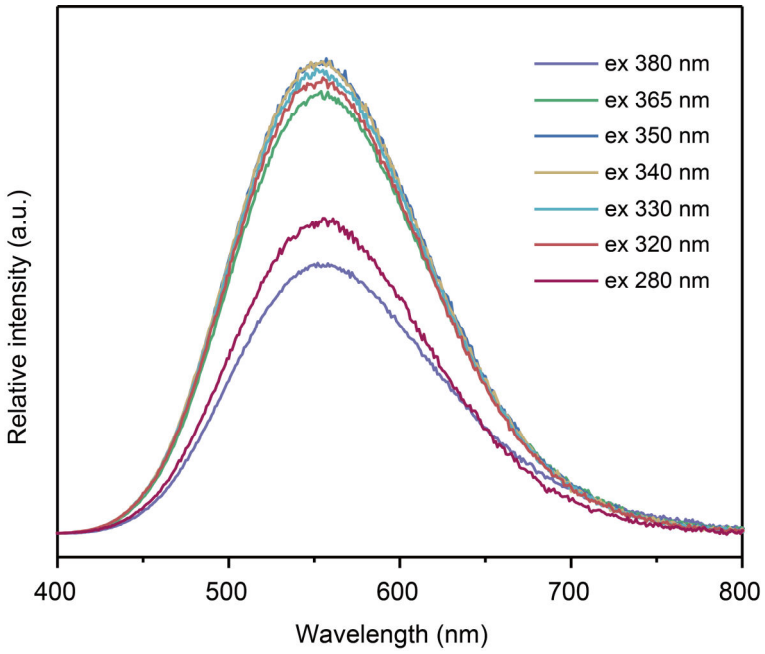

Figure S18. Emission spectra of $Bzmim_3SbCl_6$ at different excitation wavelengths.

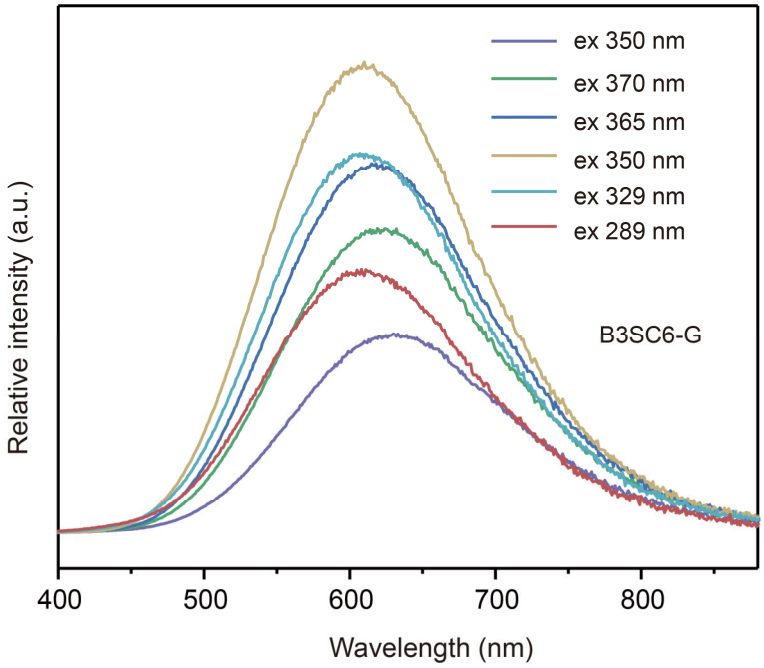

Figure S19. Excitation wavelength dependent emission spectra of $Bzmim_3SbCl_6$ glass.

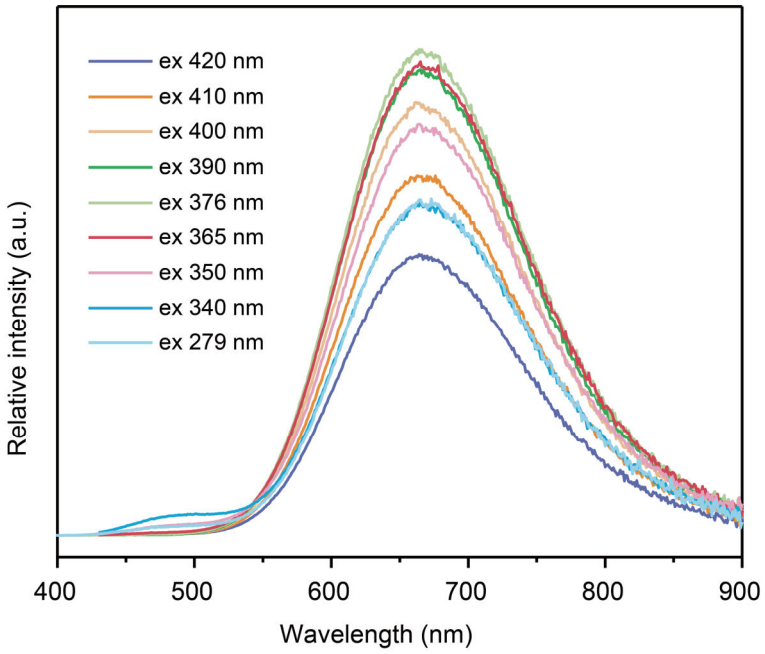

Figure S20. Emission spectra of $Bzmim_2SbCl_5$ at different excitation wavelengths.

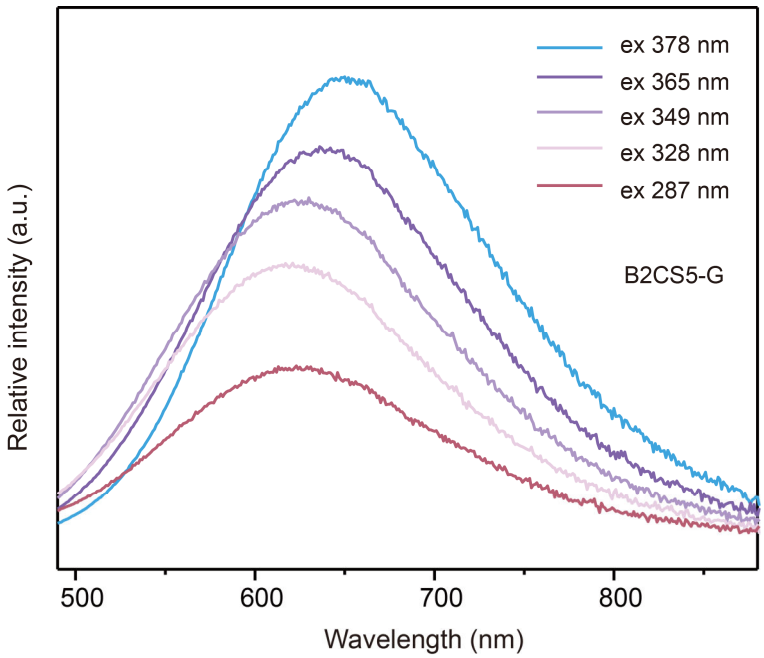

Figure S21. Excitation wavelength dependent emission spectra of $Bzmim_2SbCl_5$ glass.

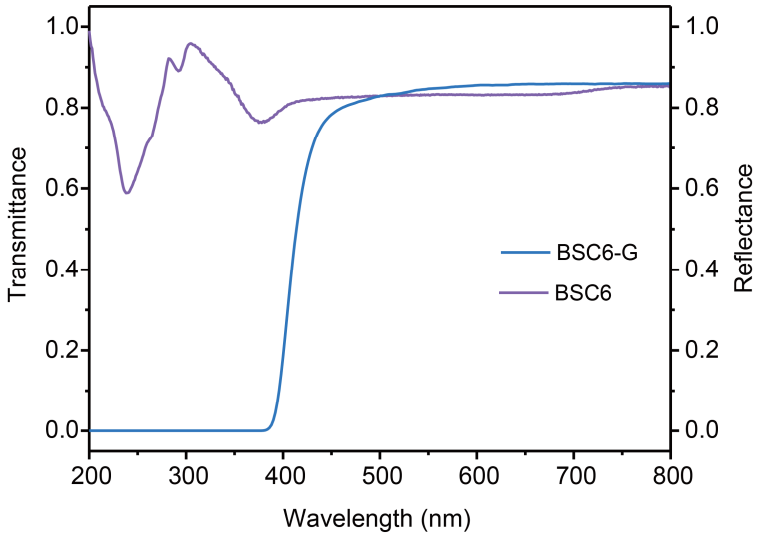

Figure S22. The UV-Vis transmittance spectrum of $Bzmim_3SbCl_6$ glass and diffuse reflection spectrum of $Bzmim_3SbCl_6$.

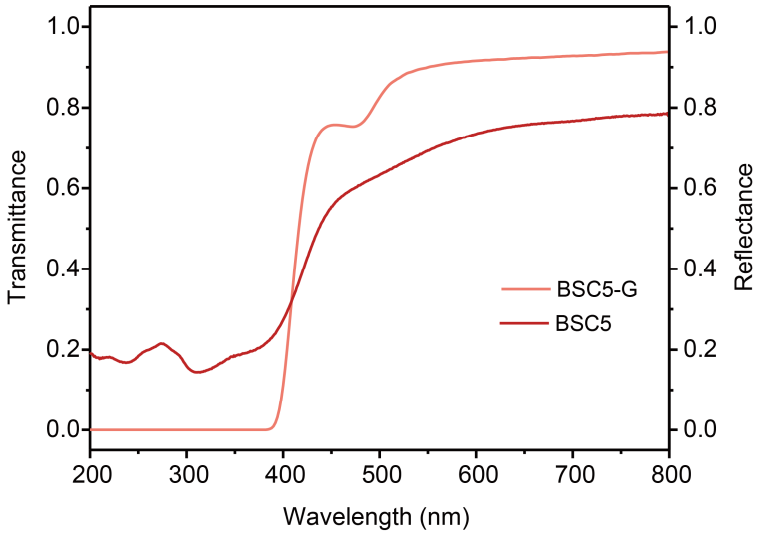

Figure S23. The UV-Vis transmittance spectrum of $Bzmim_2SbCl_5$ glass and diffuse reflection spectrum of $Bzmim_2SbCl_5$.

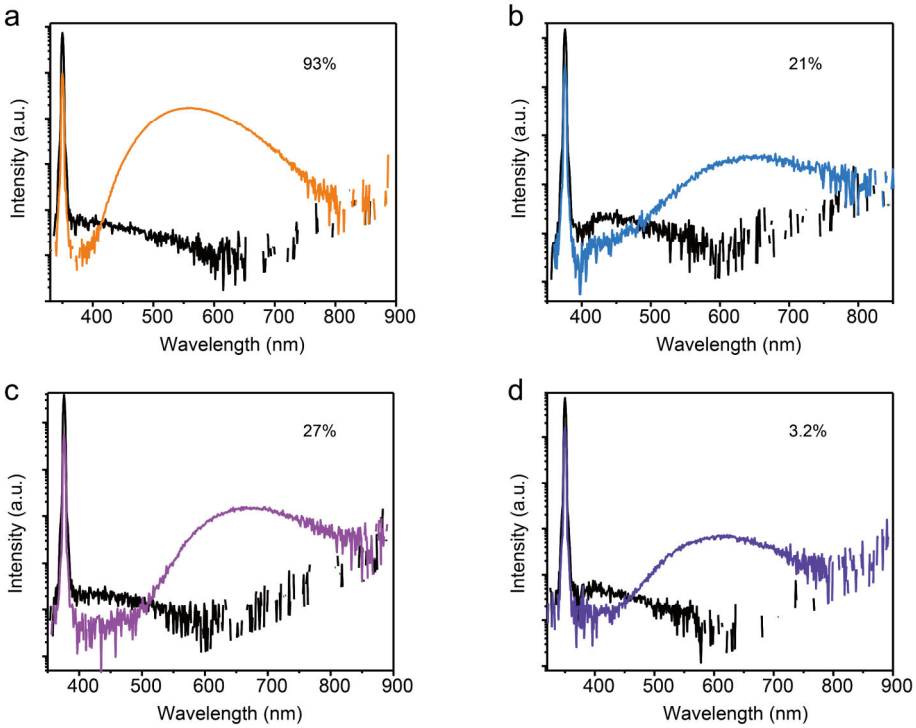

Figure S24. PLQY spectra of (a) $Bzmim_3SbCl_6$, (b) $Bzmim_3SbCl_6$ glass, (c) $Bzmim_2SbCl_5$, and (d) $Bzmim_2SbCl_5$ glass.

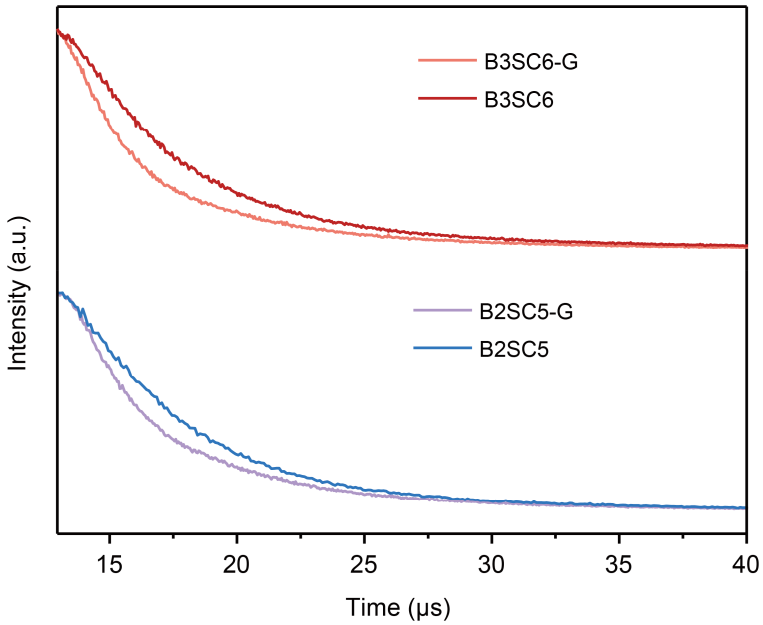

Figure S25. Fluorescence decay curves of $Bzmim_3SbCl_6$ glass, $Bzmim_3SbCl_6$, $Bzmim_2SbCl_5$ glass, and $Bzmim_2SbCl_5$.

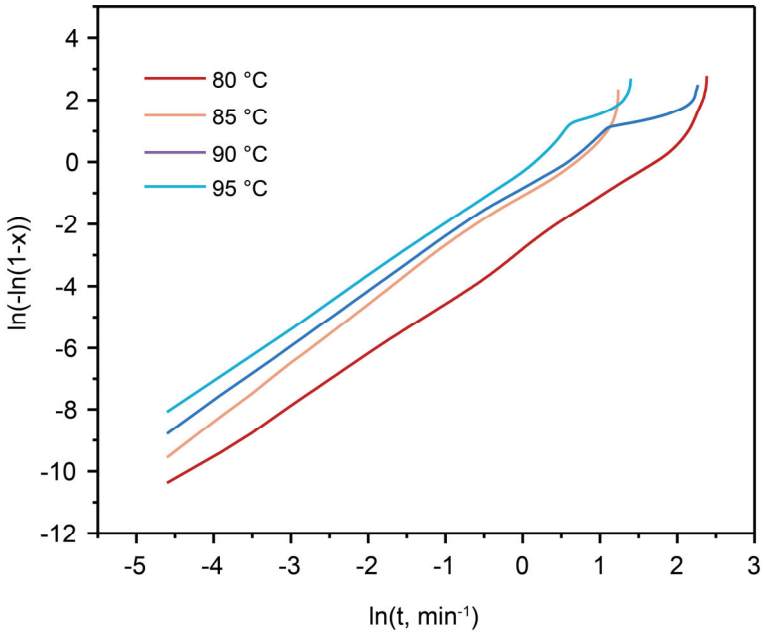

Figure S26. Plots of In(-In(1-x)) vs In(t), where x is the crystallization fraction of $Bzmim_3SbCl_6$ glass, t is the time.

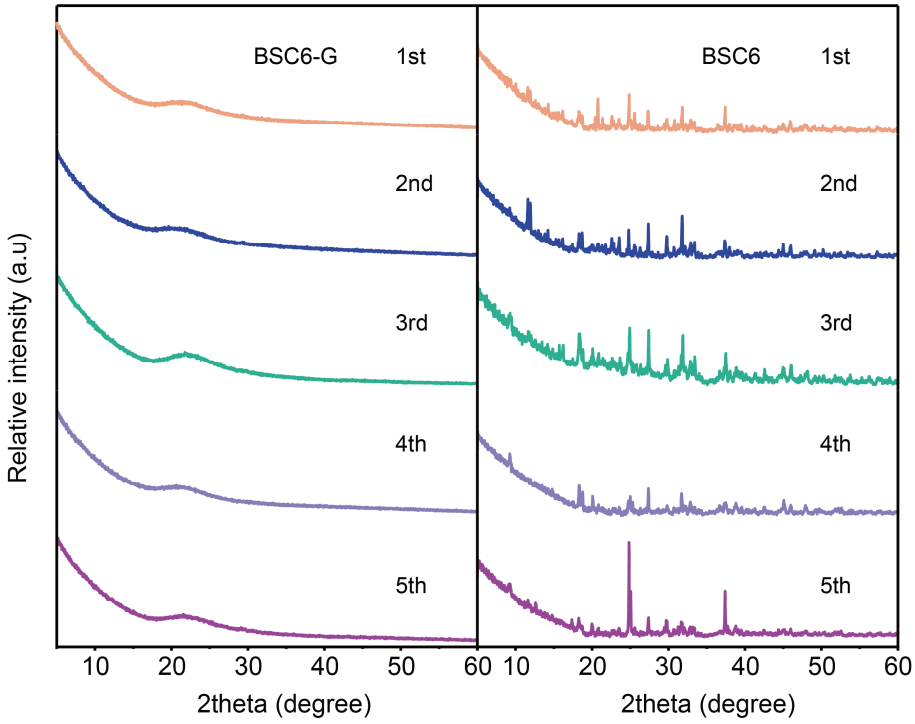

Figure S27. XRD patterns of $Bzmim_3SbCl_6$ glass (left) and $Bzmim_3SbCl_6$ (right) under five cycles of crystal-glass transformation process.

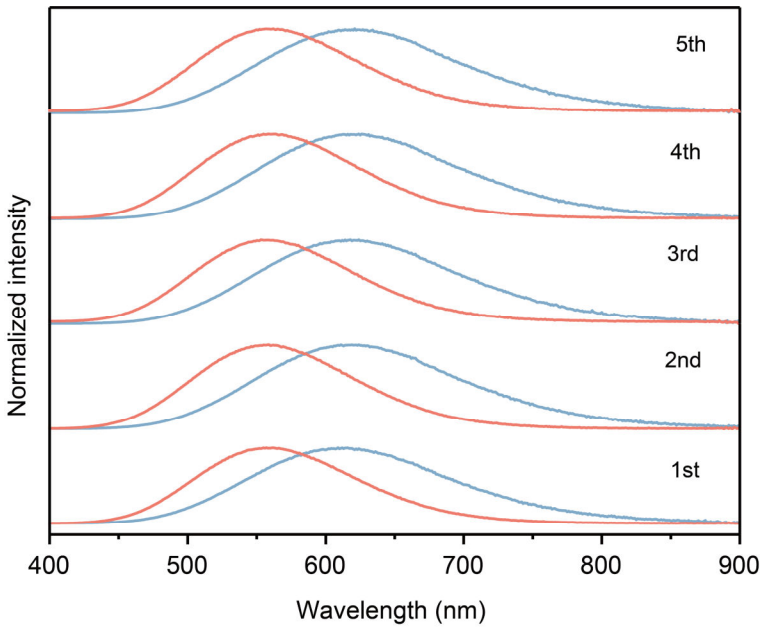

Figure S28. Emission spectra of $Bzmim_3SbCl_6$ glass (blue line) and $Bzmim_3SbCl_6$ (red line) under five cycles of crystal-glass transformation process.

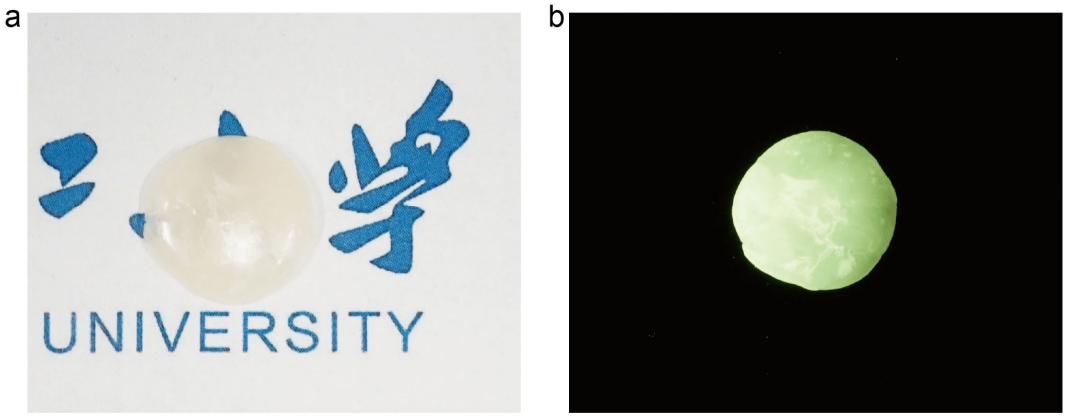

Figure S29. Photograph of $Bzmim_3SbCl_6$ glass after thermal treatment under (a) daylight and (b) 365 nm UV light.

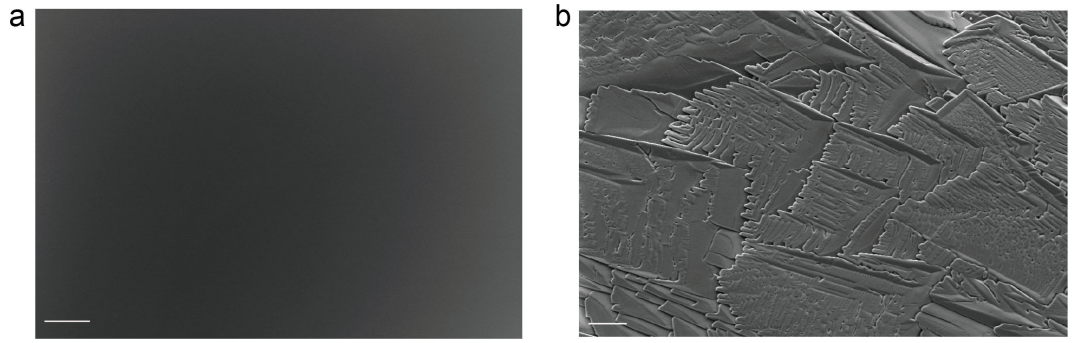

Figure S30. (a) SEM images of $Bzmim_2SbCl_5$ glass. (b) SEM images of $Bzmim_2SbCl_5$ glass ceramic. The scale bar is 30 μm.

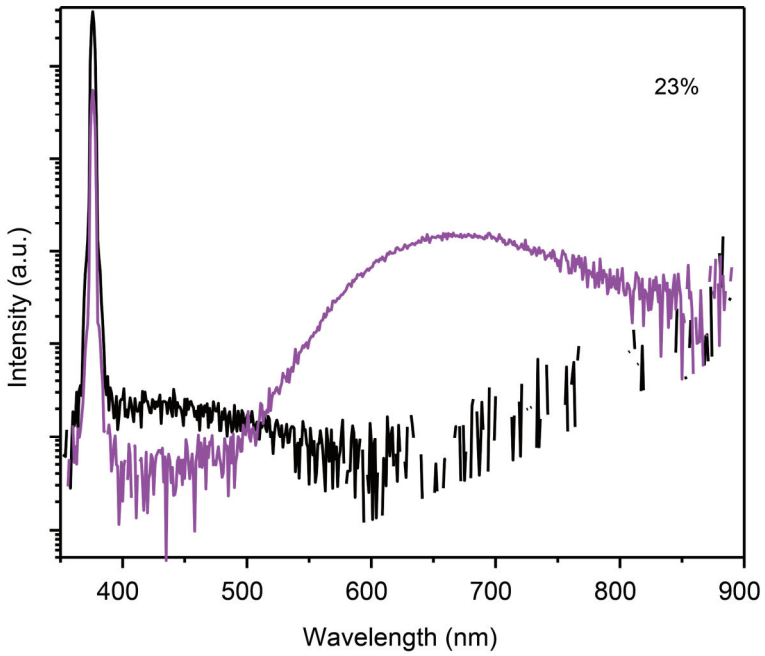

Figure S31. PLQY spectra of $Bzmim_2SbCl_5$ glass ceramic.

Table S1. Crystal data and structure refinement for $Bzmim_3SbCl_6$.

Formula	C33 H39 Cl6 N6 Sb
Temperature (K)	150.00
Formula Weight	854.18
Crystal system	monoclinic
Space group	$P2_1$
a [Å]	9.7360(6)
b [Å]	26.6108(15)
c [Å]	14.4804(10)
α [°]	90
β [°]	91.792(4)
γ [°]	90
V [Å^3]	3751.6 (4)
Z	4
*D*c [g cm^{-3}]	1.513
Radiation, *λ* ([Å]	1.34138
*R*int	0.0585
*R*1 [$I > 2\sigma(I)$] [a)]	0.0685
*wR*2 [$I > 2\sigma(I)$] [b)]	0.1679
*R*1 (all data)	0.0854
*wR*2 (all data)	0.1821
GOF	1.042

a) $R1 = \Sigma||Fo| - |Fc||/\Sigma|Fo|$; b) $wR2 = [\Sigma w(Fo^2 - Fc^2)^2/\Sigma w(Fo^2)^2]^{1/2}$.

Table S2. Crystal data and structure refinement for $Bzmim_2SbCl_5$.

Formula	C44 H52 Cl10 N8 Sb2
Temperature (K)	150 K
Formula Weight	1290.93
Crystal system	tetragonal
Space group	$I\bar{4}$
a [Å]	17.5697(15)
b [Å]	17.5697(15)
c [Å]	8.7813(10)
α [°]	90
β [°]	90
γ [°]	90
V [Å^3]	2710.7(6)
Z	2
*D*c [g cm^{-3}]	1.582
Radiation, *λ* [Å]	1.34138
*R*int	0.0585
*R*1 [$I > 2\sigma(I)$] [a)]	0.0643
*wR*2 [$I > 2\sigma(I)$] [b)]	0.1684
*R*1 (all data)	0.1051
*wR*2 (all data)	0.1917
GOF	1.066
Flack parameter	-0.017(10)

a) $R1 = \Sigma||Fo| - |Fc||/\Sigma|Fo|$; b) $wR2 = [\Sigma w(Fo^2 - Fc^2)^2/\Sigma w(Fo^2)^2]^{1/2}$.

Table S3. List of hydrogen bonds in $Bzmim_3SbCl_6$.

	Bond	Distance [Å]	Angle [°]
Sb1	C2-H2···Cl1	2.6822	133.018
	C15-H15A···Cl1	2.6680	163.664
	C33-H33B···Cl1	2.6538	171.581
	C56-H56···Cl1	2.7299	142.712
	C54-H54···Cl2	2.8835	158.200
	C44-H44B···Cl3	2.625	133.635
	C48-H48B···Cl3	2.6552	137.387
	C15-H15B···Cl4	2.6857	166.880
	C33-H33C···Cl4	2.8804	164.834
	C66-H66A···Cl4	2.7638	157.343
	C3-H3···Cl5	2.6921	151.331
	C56-H56···Cl6	2.8523	125.748
	C65-H65···Cl6	2.7004	156.865
	C23-H23···Cl6	2.7901	1447.329
Sb2	C57-H57···Cl7	2.8205	131.227
	C37-H37B···Cl7	2.6517	156.896
	C55-H55B···Cl7	2.7164	163.420
	C18-H18···Cl7	2.8612	130.743
	C1-H1···Cl7	2.5721	140.150
	C34-H34···Cl8	2.7368	137.929
	C37-H37A···Cl8	2.7995	150.335
	C26-H26A···Cl9	2.8581	143.417
	C22-H22B···Cl10	2.7683	149.194
	C24-H24···Cl10	2.8437	154.297
	C6-H6···Cl11	2.6499	157.963
	C45-H45···Cl11	2.5760	155.07
	C1-H1···Cl11	2.8848	130.787
	C44-H44A···Cl12	2.6219	168.430
	C35-H35···Cl12	2.8335	162.612
	C58-H58···Cl12	2.7686	137.641

Table S4. List of hydrogen bonds in $Bzmim_2SbCl_5$.

	Bond	Distance [Å]	Angle [°]
Sb1	C3-H11B···Cl2	2.6106	165.977
	C3-H11B···Cl2	2.6106	165.977
	C3-H11B···Cl2	2.6106	165.977
	C3-H11B···Cl2	2.6106	165.977
	C1-H1···Cl1	2.8274	143.859

	C1-H1···Cl1	2.8274	143.859
	C1-H1···Cl1	2.8274	143.859
	C1-H1···Cl1	2.8274	143.859
Sb2	C11-H11C···Cl3	2.8493	167.001
	C2-H2···Cl3	2.7623	136.045
	C11-H11C···Cl3	2.8493	167.001
	C2-H2···Cl3	2.7623	136.045
	C11-H11C···Cl3	2.8493	167.001
	C2-H2···Cl3	2.7623	136.045
	C11-H11C···Cl3	2.8493	167.001
	C2-H2···Cl3	2.7623	136.045
	C3-H3···Cl4	2.5570	171.221
	C3-H3···Cl4	2.5570	171.221
	C3-H3···Cl4	2.5570	171.221
	C3-H3···Cl4	2.5570	171.221

Table S5. T_g/T_m and T_m for the materials highlighted in Figure 3c.

Material	T_g/T_m	T_m [K]	Ref
B2O3	0.76	723	1
SiO2	0.73	2003	2
PMMA	0.77	513	3
CP	0.72	427	4
ZIF62	0.84	708	5
Water	0.5	273	6
$Bzmim_3SbCl_6$	0.74	409	this work
$Bzmim_2SbCl_5$	0.77	379	this work

Table S6. Summaries of reported T_g, T_m and T_g/T_m in Sb based metal halide hybrid glasses.

Compound	T_m	T_g	T_g/T_m	Ref
$(S\text{-}2\text{-}HMM)_3SbCl_6$	140	22	0.71	7
$Bzmim_3SbCl_6$	137.9	32.3	0.74	This work

$(ETP)_2SbCl_5$	149	38	0.74	8
$(MEP)_2SbCl_5$	214	60	0.68	8
$(BUP)_2SbCl_5$	140	47	0.77	8
$(BTP)_2SbCl_5$	226	78	0.70	8
$Bmim_2SbCl_5$	76.2	-20	0.72	This work
$Bzmim_2SbCl_5$	106.2	22	0.77	This work

Table S7. Fitting results of Avrami parameters and crystallization rates for $Bzmim_3SbCl_6$ glass at measurement temperatures.

Temperature (℃)	80	85	90	95
k (s^{-1})	0.001016	0.005474	0.007063	0.013227
n	1.63	1.92	1.77	1.68

Reference

[1] E. D. Zanotto and D. R. Cassar, *Sci. Rep.*, 2017, **7**, 43022.

[2] G. N. Greaves and S. Sen, *Adv. Phys.*, 2007, **56**, 1-166.

[3] U. Ali, K. J. B. Abd Karim and N. A. Buang, *Polym. Rev.*, 2015, **55**, 678-705.

[4] T. D. Bennett, Y. Yue, P. Li, A. Qiao, H. Tao, N. G. Greaves, T. Richards, G. I. Lampronti, S. A. T. Redfern, F. Blanc, O. K. Farha, J. T. Hupp, A. K. Cheetharm and D. A. Keen, *J. Am. Chem. Soc.,* 2016, **138**, 3484-3492.

[5] A. Qiao, T. D. Bennett, H. Tao, A. Krajnc, G. Mali, C. M. Doherty, A. W. Thornton, J. C. Mauro, G. N. Greaves and Y. Yue, *Sci. Adv.,* 2018, **4**, eaao6827.

[6] G. P. Johari, A. Hallbrucker and E. Mayer, *Nature,* 1987, **330**, 552-553.

[7] M. Yin, B. Li, Z. Yi, Y. Zhang, Z. Xia and Y. Xu, *Chem. Commun.*, 2023, **59**, 11361-11364.

[8] W. Wang, C.-D. Liu, X.-B. Han, C.-Q. Jing, C.-Y. Chai, C.-C. Fan, M.-L. Jin, J.-M. Zhang and W. Zhang, *ACS Mater. Lett.*, 2024, **6**, 203-211.